Multispectral confocal microendoscope for *in vivo* and *in situ* imaging

Houssine Makhlouf
Arthur F. Gmitro
Anthony A. Tanbakuchi
Josh A. Udovich
Andrew R. Rouse
University of Arizona
Department of Radiology
P. O. Box 245067
Tucson, Arizona 85724

Abstract. We describe the design and operation of a multispectral confocal microendoscope. This fiber-based fluorescence imaging system consists of a slit-scan confocal microscope coupled to an imaging catheter that is designed to be minimally invasive and allow for cellular level imaging *in vivo*. The system can operate in two imaging modes. The grayscale mode of operation provides high resolution real-time *in vivo* images showing the intensity of fluorescent signal from the specimen. The multispectral mode of operation uses a prism as a dispersive element to collect a full multispectral image of the fluorescence emission. The instrument can switch back and forth nearly instantaneously between the two imaging modes (less than half a second). In the current configuration, the multispectral confocal microendoscope achieves 3-μm lateral resolution and 30-μm axial resolution. The system records light from 500 to 750 nm, and the minimum resolvable wavelength difference varies from 2.9 to 8.3 nm over this spectral range. Grayscale and multispectral imaging results from *ex-vivo* human tissues and small animal tissues are presented. © *2008 Society of Photo-Optical Instrumentation Engineers.* [DOI: 10.1117/1.2950313]

Keywords: multispectral confocal microendoscope; *in vivo* imaging; cellular level imaging; fiber-based fluorescence.

Paper 07473R received Nov. 27, 2007; revised manuscript received Feb. 3, 2008; accepted for publication Feb. 6, 2008; published online Jul. 10, 2008.

1 Introduction

In vivo confocal microendoscopes provide high resolution cellular imaging in a relatively small package. This minimally invasive technique provides instant visualization of tissue and allows pathologists to make a diagnosis *in situ* without having to use traditional tissue extraction biopsy methods. Confocal microendoscopy can be performed in reflectance[1,2] or fluorescence[3–8] modes. However, most confocal microendoscopes are designed for fluorescence imaging and record the integrated fluorescence signal in a single image. Confocal microendoscopy has been used for the detection and diagnosis of diseases in a broad variety of organs such as cervix,[2] colon,[3] oral cavity,[7] esophagus,[8] and ovary.[9]

We have previously reported on the design and demonstration of several confocal microendoscope systems. The grayscale imaging mode of our confocal microendoscope has shown significant promise as a diagnostic instrument, and a laparoscopic version is currently being used to investigate ovarian cancer in an *in vivo* clinical trial. The details of the grayscale confocal microendoscope, and the general concept of multispectral confocal microendoscopy, have been presented in previous publications.[10–14] Our current confocal microendoscope is a modification of a previous system, in which a new multispectral imaging mode has been implemented. The multispectral mode of operation provides additional diagnostic information by measuring the fluorescence signal as a

function of wavelength. To our knowledge, there is only one other confocal microendoscope capable of spectral data acquisition.[15] This system provides full spatial resolution in two distinct spectral ranges and also provides full spectral information averaged over the entire field of view. Our multispectral confocal microendoscope can provide full spectra associated with every image point. Applications for the multispectral confocal microendoscope include the detection of disease by providing unique diagnostic information using tissue or organelle-specific fluorophores with specific spectral properties.

The purpose of this work is to describe the design of the multispectral imaging mode of our confocal microendoscope and demonstrate the capabilities of the system as a clinical diagnostic instrument. First, the current grayscale mode of operation is described in terms of system design, performance, and results. Then, a detailed description of the multispectral mode of operation is given, including the tools associated with presenting the multispectral data. Finally, preliminary multispectral imaging results obtained from biological specimens are presented.

2 Design of the System

2.1 *Grayscale Imaging Mode*

Figure 1 shows the layout of the confocal microendoscope in grayscale mode.[11] A 488-nm diode-pumped solid-state laser (Coherent, Santa Clara, California) is used as the excitation

---

Address all correspondence to Andrew R. Rouse, Department of Radiology, University of Arizona, P.O. Box 245067, Tucson, Arizona 85724-5067. Tel: 520-626-5894; Fax: 520-626-3893; E-mail: rouse@u.arizona.edu.
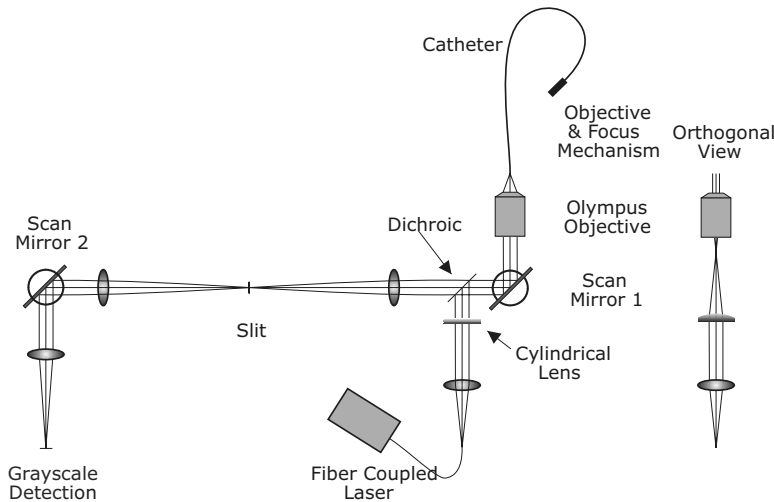
Fig. 1 Layout of the confocal microendoscope. The orthogonal view shows the illumination path from the direction for which the cylindrical lens has optical power.

source. A line of illumination, formed by spherical and cylindrical lenses, is coupled into the proximal end of the catheter by a 10× microscope objective (Leeds Precision Instruments, Minncapolis, Minnesotre). A 30,000 element coherent fiber bundle (Sumitomo Electric USA, Torrance, California) transmits the illumination profile to the distal end of the fiber, which is imaged into the tissue by a miniature objective. A focus mechanism enables focus control down to 200 μm below the tissue surface. Scan mirror 1 sweeps the illumination profile across the field of view. Fluorescence light from the sample is collected back into the system via the miniature objective and fiber bundle, and separated from the reflected illumination by a dichroic beamsplitter (Chroma Technology Corporation, Rockingham, Vermont). The fluorescence light is then focused onto the confocal slit aperture, which rejects light from out-of-focus planes and provides the optical sectioning (confocal) capability of the system. A second scan mirror, placed between two lenses, images the light passing through the confocal slit onto a charge-coupled device (CCD) camera (Photometrics, Tucson, Arizona). The two scan mirrors are synchronized to provide correspondence between the illumination profile in the tissue and the detection profile on the CCD. Figure 2 shows a picture of the confocal microendoscope system.[11]

In operation, the distal end of the catheter is placed in contact with the sample and a small amount of fluorescent dye ($\approx$10 μL per image) is delivered to the area of interest. The user adjusts the focus of the catheter, and images are collected by the computer for processing and/or subsequent analysis.

2.2 Multispectral Imaging Mode

2.2.1 Layout of the multispectral channel

The layout of the multispectral mode is shown in Fig. 3. The novel design requires nothing more than a 45-deg BK7 prism (OptoSigma, Santa Ana, California) located away from the optical axis. The off-axis position enables us to leave the prism in a fixed position that does not disturb the beam path in grayscale mode. The system switches rapidly between the two modes of operation (grayscale and multispectral) in less than

half a second. To switch from grayscale to multispectral imaging mode, the computer-controlled galvo mirror (scan mirror 2) is rotated to a fixed position. The fluorescence signal, reflected by this mirror, is dispersed by the prism and focused on the CCD camera at different spatial locations according to wavelength. For each position of the first scan mirror (scan mirror 1), the system records the 2-D light signal pattern on the CCD, which has one spatial dimension (along the slit direction) and one spectral dimension (perpendicular to the slit direction). Repeating this process (reading out a frame of data from the 2-D detector) for every position of the first scan mirror allows one to reconstruct a 3-D data cube that consists of two spatial dimensions and one spectral dimension. The prism is adjusted for minimum deviation to simplify the design and the theoretical modeling of the system. This configuration also yields a simple way of aligning the prism in the system. The orientation of the prism and the incidence angle of the beam on the prism entrance face are such that the central wavelength, 600 nm, is imaged to the center of the
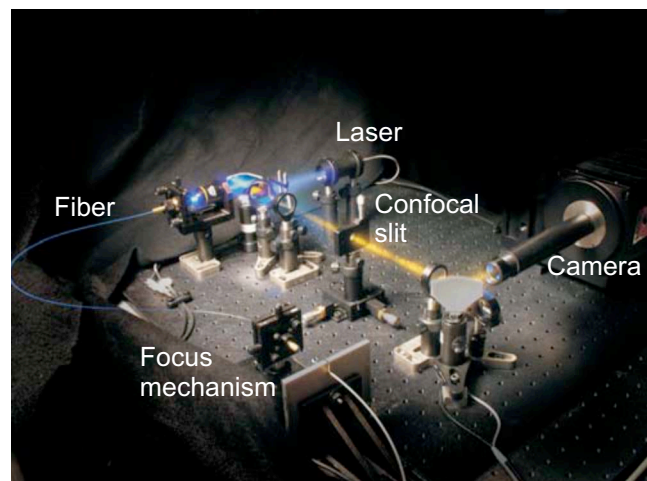

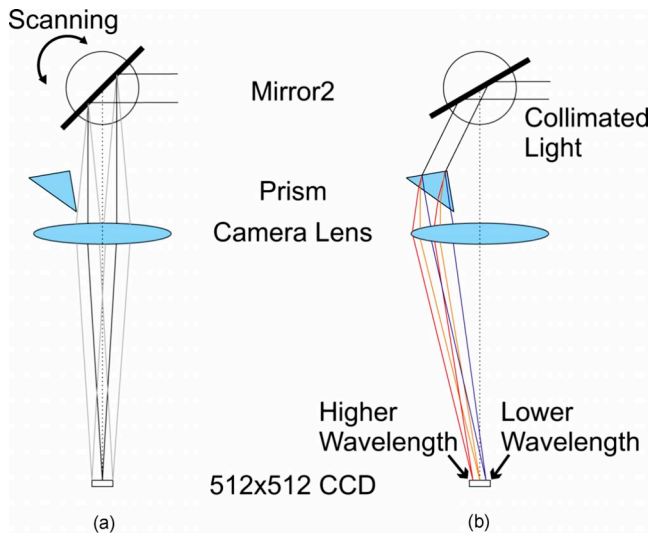**Fig. 2** Photograph of the confocal microendoscope.

Fig. 3 Grayscale (a) and multispectral (b) beam paths. Shorter wavelengths exit the prism with the largest deviation angle. Dispersed light is focused on the CCD camera. The position on the detector is directly related to wavelength. Mirror 2 is stationary in the multispectral mode of operation.

CCD detector at minimum deviation. In other words, the 600-nm signal comes out of the prism parallel to the optical axis. The diameter of the camera lens (180-mm focal length and 60-mm entrance pupil) is large enough to collect the dispersed beam from the prism.

A calibration procedure employing a theoretical dispersion profile is used to map detector pixels to wavelength. The details of the calibration procedure are discussed in the next section.

2.2.2 Tools used in the multispectral mode

Multispectral data cube. As discussed in the previous section, the camera records one spatial dimension and one spectral dimension for each orientation of scan mirror 1. Figure 4 shows images obtained from three different positions of scan

mirror 1. The amplitude of the mirror is set to sweep the illumination line over the full field of the fiberoptic imaging bundle. The frequency of the mirror is adjusted so that the camera acquires 512 frames in a single sweep. Collection of a full dataset takes roughly 6 s and results in a data cube consisting of 512×512 spatial pixels and 150 spectral pixels.

Display software. Custom software was developed to aid in the display and analysis of the 3-D multispectral data cube. Figure 5 shows a screenshot of this software when the confocal microendoscope was back illuminated by a white light source filtered down to a 695- to 705-nm spectral range. The main window shows the 2-D spatial distribution of the sample at a specific wavelength, while the side windows show the distribution of one spatial dimension as a function of wavelength. At the bottom, the software displays the full spectrum associated with the current cursor location.

The program is fully interactive; a mouse click anywhere on the 2-D image in the main window will plot the spectrum associated with that point and update the side windows to show the spectral information along the horizontal and vertical lines through the selected point. A mouse click on one of the side windows will display, in the main window, the 2-D spatial distribution of the 3-D data cube at the specified wavelength.

Wavelength calibration procedure. To plot the spectrum associated with a given spatial point in the image (bottom plot of the display program), it is necessary to determine the relationship between CCD pixel position and wavelength.

The fixed tilt angle θ_m of mirror 2 and the rotation angle θ_p of the prism define the incident angle θ_i of the light on the prism surface. Given the incident angle θ_i of light on a prism of wedge angle α and index of refraction n, the deviation angle D produced by the prism is given by
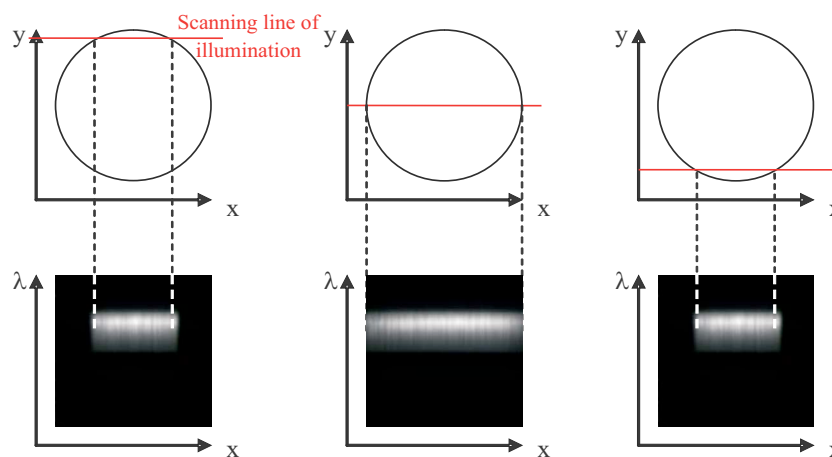

Fig. 4 Relationship between spatial location (top graphs) and spectral frames (bottom graphs). The lines in the upper images represent the slit illumination profile as it scans across the *y*axis of the field of view. The lower images show the dispersion introduced by the prism at the selected scanning positions.
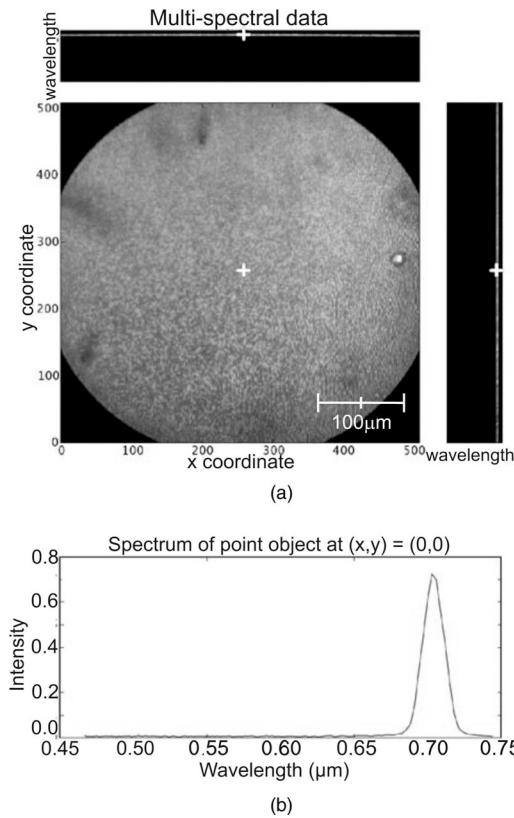
Fig. 5 Image of the illuminated fiber bundle using a lamp with a 700-nm optical filter. (a) Cross-section planes of the data cube and (b) spectrum of the image point indicated by a white cross. The intensity is unitless because it is scaled relatively to the maximum intensity in the image.

$$D(\lambda) = \theta_i - \alpha + \sin^{-1}(\sin\alpha\sqrt{n(\lambda)^2 - \sin^2\theta_i} - \sin\theta_i\cos\alpha). \tag{1}$$

The deviation angle varies with wavelength because the index of refraction of the prism is wavelength dependent. This property is well described by the Sellmeier equation for the BK7 glass in the prism. The deviation D and the angles θ_m and θ_p are related to the incident angle θ_c of the light entering the camera. The pixel offset on the CCD is given by the relationship

$$Np = f_c \tan\theta_c, \tag{2}$$

where N is the number of pixels offset from the optical axis, p is the pixel size, f_c is the focal length of the camera lens, and θ_c is the angle of incidence on the camera lens. Using Eq. (2), the Sellmeier equation, and the various parameters of the system, it is possible to numerically invert Eq. (1) to determine wavelength as a function of pixel offset or $\lambda(N)$. Through this numerical inversion, a lookup table can be generated to precisely convert CCD pixel offset to wavelength.

In practice, a multispectral calibration image is collected using a narrowband optical filter (e.g., Fig. 5). The calibration routine looks for the maximum intensity in the reference 3-D data cube and records its spectral value in terms of pixel number on the CCD. The program then uses this information, along with a pixel offset lookup table, derived by the method just described, to determine the correspondence between wavelength and pixel position for the entire CCD.

3 System Performance and Results

3.1 Performance of the System

The slit-scan confocal microendoscope uses a catheter based on a fiber optic imaging bundle. The pixilated fiber bundle acts as a sampling system with a 3-μm center-to-center pixel spacing. In terms of the spatial resolution, the effect of the fiber bundle may be modeled as a convolution of the object with the pixel function. This model predicts a theoretical tissue-space lateral resolution of 1.9 μm and a theoretical tissue-space axial resolution of 20 μm using our 3-mm-diam distal objective with a magnification of 1.5 from tissue to fiber.[13] The confocal microendoscope provides the same spatial resolution in both multispectral and grayscale imaging modes. Spatial resolution was measured, based on the full width at half maximum (FWHM) of the point spread function (PSF), by Rouse et al.[10] to be roughly 3-μm lateral and 30-μm axial resolution over a field of view of 450 μm. The confocal microendoscope is able to focus down to a depth of 200 μm in the tissue. For the experimental results shown thereafter, the depth of observation is not precisely known. Images were acquired by focusing on the tissue surface. The optical power incident on the surface of the tissue is typically less than 1 mW. This yields a power density over the field of view of roughly 630 mW/cm^2.

The camera used in the multispectral confocal microendoscope is a Photometrics Cascade II CCD (Photometrics, Tucson, Arizona) with a 512×512 detector matrix. Each detector element is 16×16 μm. The camera is capable of recording 30 images per second, so a 3-D dataset consisting of 150 spectral samples is collected in about 6 s. Methods to increase the collection speed are presented in Sec. 4.

Spectral resolution is defined as the minimum resolvable wavelength difference. In our system, the theoretical spectral linewidth is determined by the convolution of the geometrical image of the slit on the detector, the camera pixel function, and the PSF of the camera lens. The theoretical FWHM of the spectral linewidth is 1.9 pixels and does not change significantly with wavelength within our spectral bandwidth. The spacing between two resolvable wavelengths is then approximately 2 camera pixels. This spacing can be correlated to a change in wavelength using the wavelength calibration procedure described. Because refractive index is a nonlinear function of wavelength, the dispersion of light through the prism is not constant. Consequently, the spectral resolution is not constant with wavelength. Our system achieves a spectral resolution of 2.9 nm at a wavelength of 500 nm and 8.4 nm at a wavelength of 750 nm. Table 1 shows the spectral resolution with respect to wavelength at intervals of 50 nm. At this stage of the system development, the recorded spectra are not corrected for the camera spectral sensitivity.

3.2 Results from Grayscale Imaging

The grayscale imaging mode of the confocal microendoscope has been used to investigate a wide variety of human and animal tissues. The results presented here were obtained through topical administration of acridine orange (AO) (Invit-

Table 1 Wavelength-dependent spectral resolution.

Wavelength (nm)	Spectral resolution (nm)
500	2.9
550	3.8
600	4.9
650	6.0
700	7.2
750	8.4

rogen, Eugene, Oregon), which is a vital dye that stains DNA and RNA. Figure 6 shows an ensemble of grayscale confocal microendoscope images obtained from excised human tissues and in a mouse[11] that was sacrificed immediately prior to an *in situ* experiment. For each biological sample, about 10 μL of AO (0.1 mg/mL of concentration) was applied to the tissue surface. Imaging was started almost immediately.

Figures 6(a) and 6(b) show results obtained from excised human ovary. One can clearly visualize significant differences between the two images. Figure 6(a) shows a uniform layer of cells, which is typical for healthy ovarian epithelium. Figure 6(b) shows an abnormal pattern of cells that is indicative of pathology. These data were histologically verified as normal for Fig. 6(a) and cancerous for Fig. 6(b).

Figures 6(c) and 6(d) show images obtained from excised human esophagus. The sample in Fig. 6(c) was diagnosed as normal squamous epithelium, while the sample in Fig. 6(d) was diagnosed as Barrett's esophagus, which is a common precursor to esophageal adenocarcinoma. The sparse punctate nuclei of Fig. 6(c) and the glandular structure of Fig. 6(d) are in agreement with the histological findings. The images presented in Figs. 6(a)–6(d) were collected over several experiments and as such, the absolute brightness and contrast between images should not be compared.

Figures 6(e) and 6(f) show images of mouse peritoneal wall and liver, respectively. The animal used in this experiment was considered healthy, and no specific abnormalities were observed in the images.

3.3 Results from Multispectral Imaging

Preliminary multispectral imaging experiments were performed using a phantom containing a mixture of 15-μm-diam microspheres (Invitrogen, Eugene, OR) with different spectral properties. Figure 7 shows images of these microspheres at two different spectral planes of the multispectral data cube.

Some beads are visible at 639 nm (a) that are not visible at 578 nm (b). The difference in the spectra shows that two groups of microspheres are present in the sample. The first group has a peak emission around 640 nm, while the second group has a peak emission at 600 nm.

Figure 8 shows multispectral data obtained from an excised human esophagus stained with AO. This biological sample was from a patient diagnosed with Barrett's esophagus. Several drops of AO (0.1 mg/mL of concentration) were
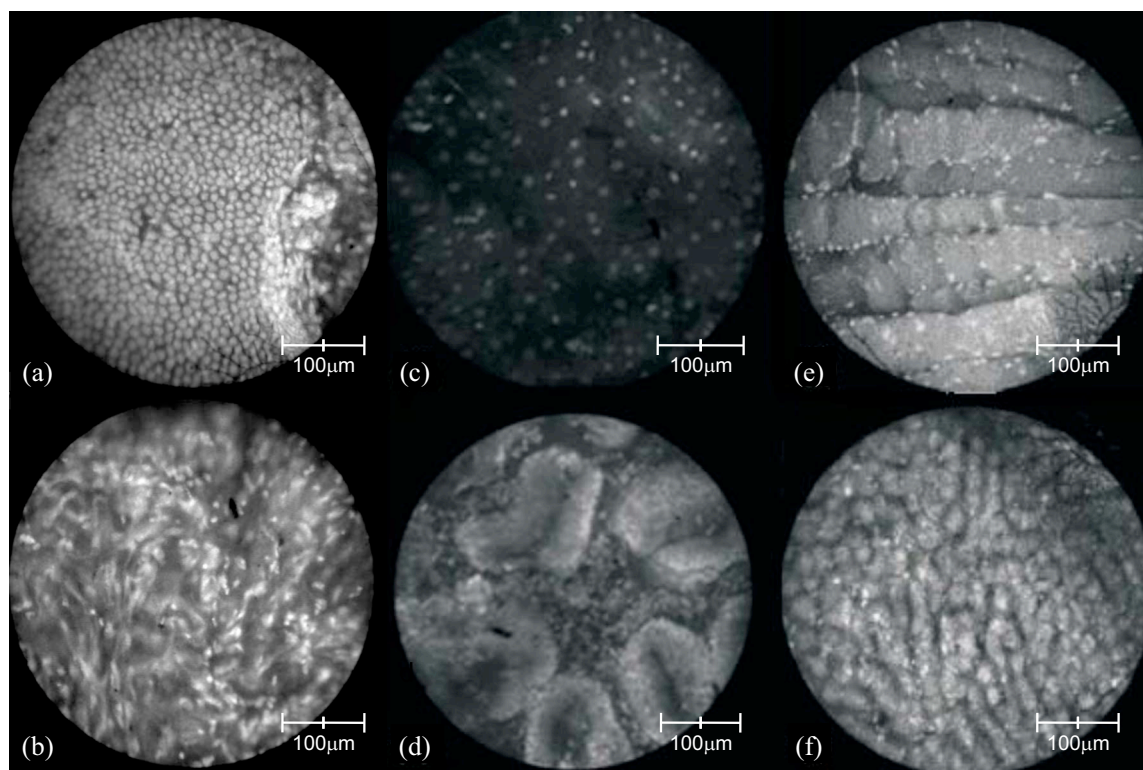

Fig. 6 Grayscale results from excised human tissues and *in situ* animal tissues. (a) Normal appearing epithelium of human ovary, (b) unusual area of human ovary, (c) normal tissue of human esophagus, (d) human Barrett's esophagus, (e) peritoneal wall of a mouse, and (f) liver of a mouse.
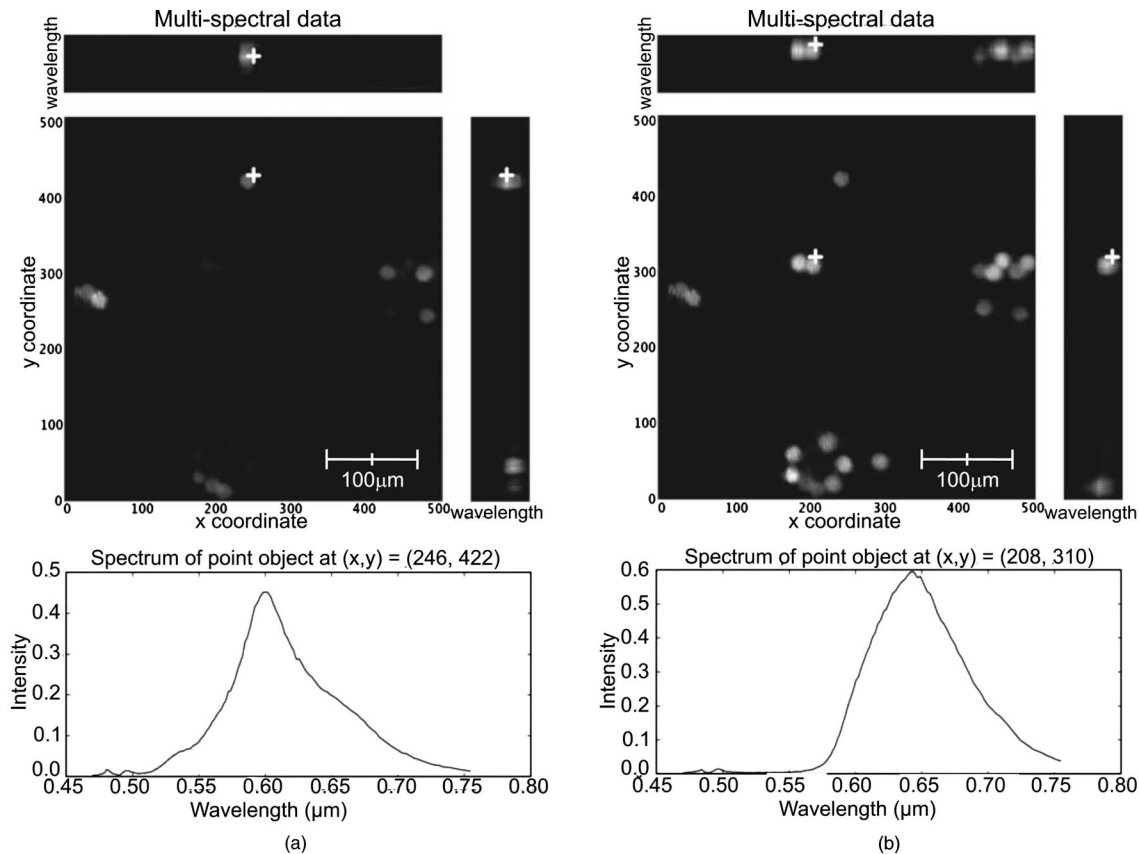
Fig. 7 Fluorescence images from 15-μm microspheres at wavelength (a) 578 nm and (b) 639 nm, and spectra associated with image point indicated by the white cross.

topically applied to the tissue. Imaging was initiated almost immediately and continued for roughly 20 min. The left image shows a low wavelength emission at 540 nm, while the right image shows a high wavelength emission at 670 nm. Different structured features are observed at the different wavelengths. This is also visible on the side windows (representing one spatial dimension as a function of wavelength), where the intensity distribution varies depending on the wavelength and exhibits two broad spectral regions of fluorescence. The spectrum at the bottom of each image is plotted for the point in the image indicated by the white cross. The presence of two distinct spectral structures is confirmed by the dual peaked spectra. Although the tissue is from a patient with Barrett's esophagus, typical glandular structures of Barrett's [see Fig. 6(d)] were not observed for this sample (not even in a slide made from this tissue and viewed with a standard microscope), and a normal-looking distribution of squamous epithelium corresponding to nuclei are visible at the low wavelength. At the high wavelength, a uniformly distributed bright region is caused by the fluorescence from cellular cytoplasm. Nuclei are still visible in the background. Some dark areas correspond to the voids left by blood vessels that were washed off in the process of biopsy. AO typically shows green fluorescence in the nuclei and red fluorescence in the cytoplasm when excited at 488 nm. However, the peak and linewidth of AO's fluorescence spectrum varies depending on the pH in the tissue and the concentrations of the solvent and other cellular structures.[16–18]

Figure 9 shows images of the peritoneal wall of a mouse stained with AO and obtained *in situ*. The mouse was sacrificed prior to the experiment and opened up to allow insertion of the catheter. A few drops of AO (0.1 mg/mL of concentration) was deposited on the peritoneal wall. We started imaging about one minute later and continued for approximately 10 min total. Again, some structures are visible at the higher wavelength (762 nm), but not at the lower wavelength (572 nm). These organelles might be lysosomes. The spectra associated with the cursor location are also shown; the spectrum on the left has a peak around 570 nm, while the spectrum on the right, corresponding to the organelles, exhibits a peak around 740 nm. Thus different aspects of the tissues are distinguishable through their emission spectra.

Figure 10 shows data obtained from a rat intestine after tagging it with DiA. DiA is a fluorophore that is used to label cytoplasmic membranes, with a peak emission at 586 nm and a peak excitation at 454 nm (Invitrogen, Eugene, Oregon). Tissues were topically stained with DiA at a concentration of 2.5 mg/mL. Different structures are observed when scanning from low to high wavelengths (from left to right in Fig. 10). The spectra associated with these structures are plotted below the corresponding images and also confirm the presence of different staining patterns. The left spectrum has a broad peak in the 610-to-640-nm range, while the spectrum in the other two images shows a broad peak in the 660-to-710-nm range.
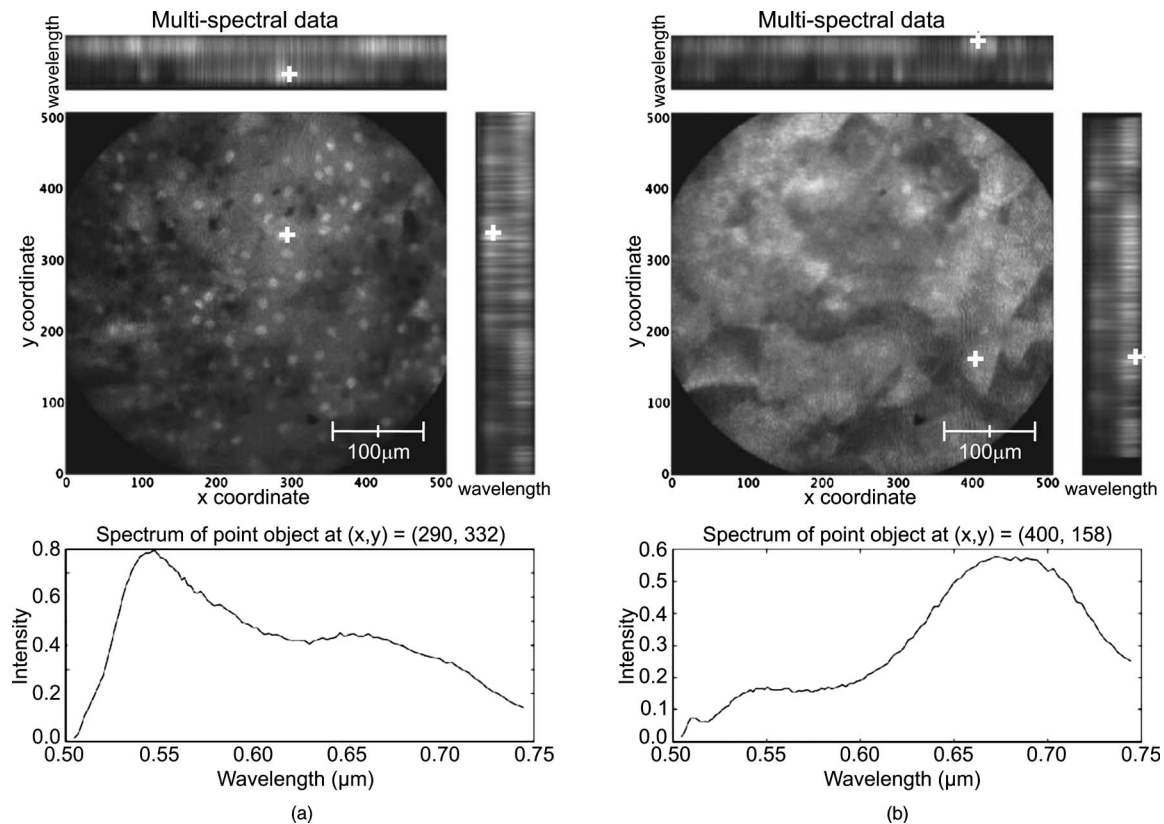
Fig. 8 Human Barrett's esophagus tissue stained with AO (a) at a low wavelength and (b) at a higher wavelength. The spectrum associated with the image point indicated by the white cross is displayed below each image.

The images demonstrate that the multispectral confocal microendoscope can differentiate different tissue types and provide high quality images across the whole field of view. Moreover, the automated data acquisition system and processing software that has been developed yield spectral information that has the potential to provide additional *in vivo* diagnostic information. As a consequence, distinct elements of a given tissue sample can be highlighted based on spectral differences in their fluorescence properties.

4 Discussion

The multispectral confocal microendoscope has been dramatically improved compared to a previous design.[12,13] The current system has fewer than half the components of the older system, making it more compact, robust, and mobile with less risk of misalignment. The reduction in complexity also increases the throughput of the system as well as the overall optical performance. The dual scan-mirror design allows the implementation of both grayscale and multispectral imaging capability using a single CCD camera. The system is capable of rapidly switching between the two imaging modes of operation simply by tilting the second scan mirror to a fixed position, scanning the first mirror more slowly, and collecting data in multiple frames.

The multispectral mode of operation was designed to collect data over a spectral range of approximately 250 nm with a spectral resolution of better than 8 nm across this range. The spectral resolution of the system could be increased by using a prism made from glass with higher dispersion. For instance, using F2 glass instead of BK7, one could theoretically achieve a spectral resolution of 1.2 nm at 500 nm and 4.3 nm at 750 nm, which is about a two-fold improvement in spectral resolution. The price to be paid is the readout of a larger area of the CCD and a roughly two-fold increase in data collection time.

There are constraints imposed by the off-axis prism design for the multispectral mode of operation. The deviated beam coming out of the prism has to fall within the entrance pupil of the camera lens, and the spread of angles caused by the prism has to remain within the angular field of view imposed by the size of the CCD and the imaging optics. A 180-mm focal length f/2.8 lens was used to satisfy these constraints. As an alternative configuration, the prism could be replaced by a diffraction grating. A higher spectral resolution could be achieved that would remain constant with respect to wavelength. However, the simple off-axis design would not work and the grating would need to be translated into the beam. This would require a more complex mechanical system and a slightly longer transition time between grayscale and multispectral imaging modes. A grating-based design would also suffer from slightly reduced light efficiency.

In the current system, collection of the full multispectral dataset takes a significant amount of time (about 6 s). Motion of the sample during data acquisition leads to image distortions. However, the contact imaging catheter is quite stable during *in vivo* experiments, which allows us to collect high
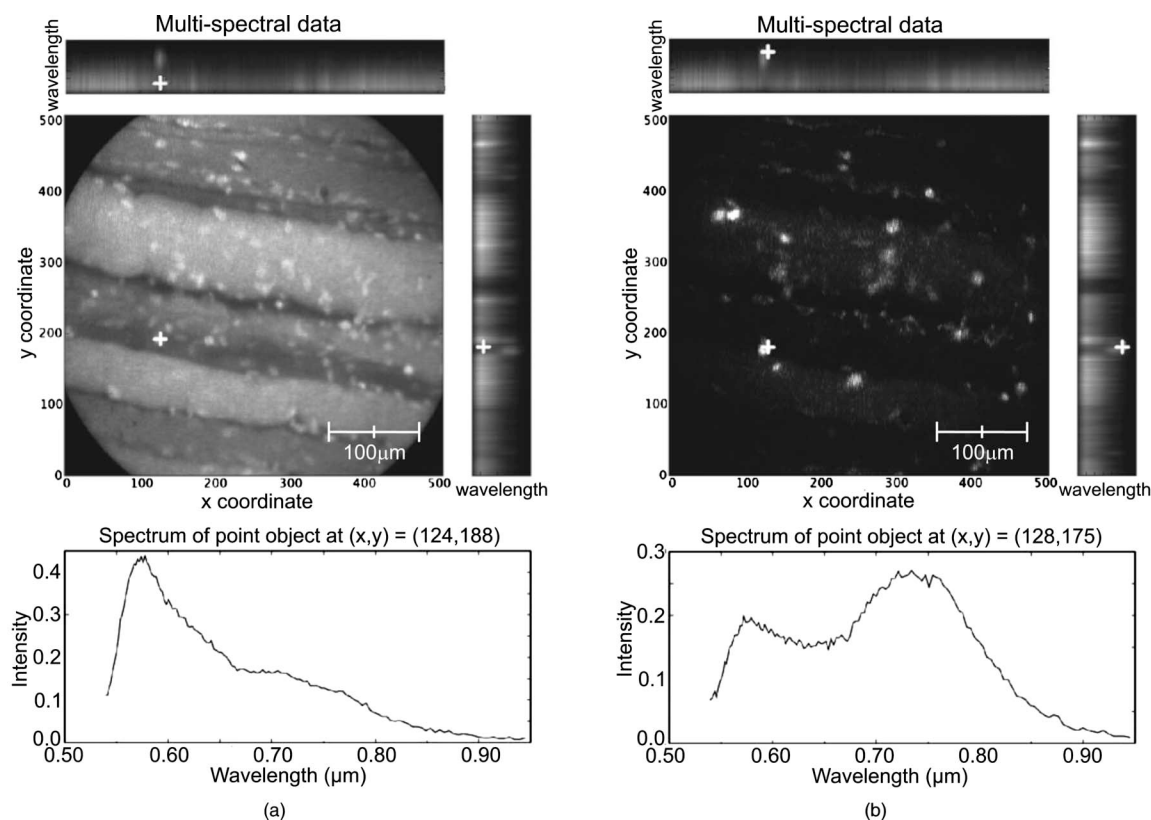
Fig. 9 *In situ* images of the peritoneal wall of a mouse stained with AO at different wavelengths, (a) 572 nm and (b) 762 nm. The spectrum associated with the image point indicated by the white cross is displayed below each image.

quality multispectral data. The speed of acquisition can be increased in several ways. One could choose a reduced number of spectral samples around a specific spectral region of interest, or set up the camera to bin in the spectral dimension.

Cameras are available (e.g., Computer Modules Incorporation, San Diego, California) that operate at several thousand frames per second. However, a shorter data collection time would lead to a decrease in signal-to-noise ratio (SNR), as-
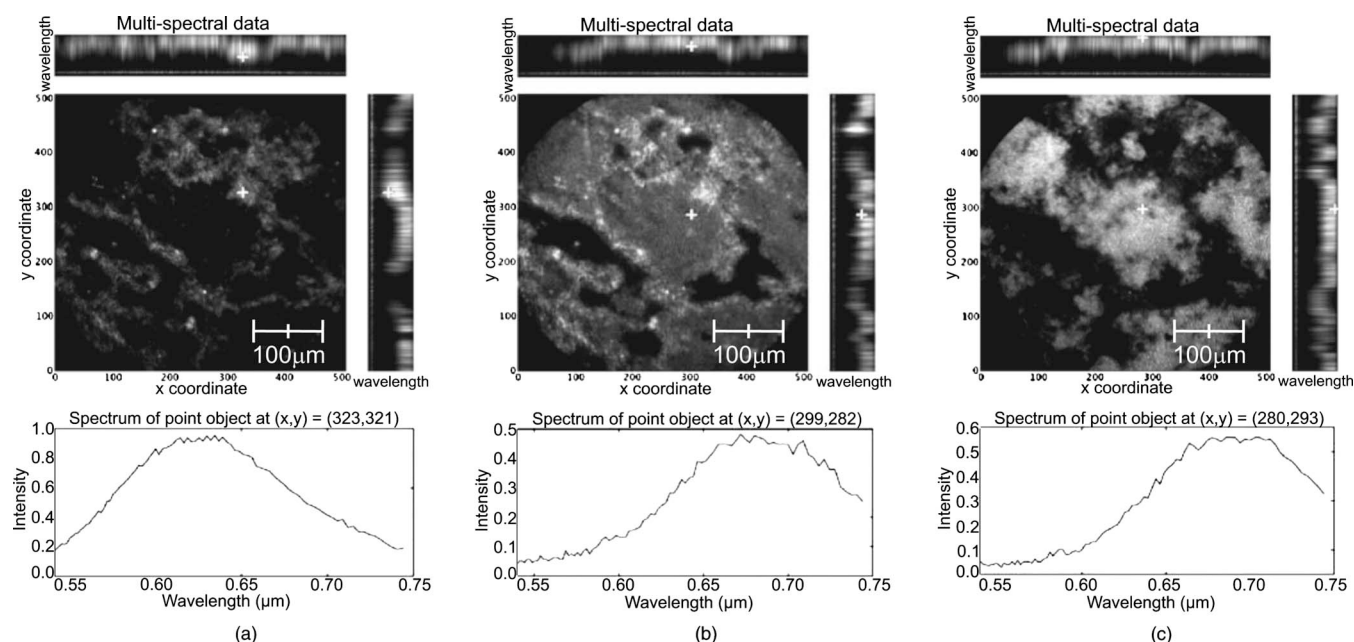

Fig. 10 Rat intestine stained with DiA at a (a) low wavelength, (b) intermediate wavelength, and (c) high wavelength.

suming the same illumination level and dye concentration. There is clearly a tradeoff between multispectral data acquisition time, motion sensitivity, and SNR that should be carefully evaluated for each specific application.

The results obtained from the multispectral mode of operation are quite promising, and further investigation of additional dyes that stain specific cellular components is warranted. The use of multiple dyes and perhaps multiple excitation sources could yield even more useful spectral information. Data postprocessing, incorporating spectral unmixing, could provide more quantitative information. Morphological changes in cellular structure could be monitored via multispectral data collection. For example, measurement of nuclear-to-cytoplasmic ratio in cells could be accomplished using dyes that label the cell nucleus and cytoplasm with different spectral emission characteristics. This could be accomplished with multiple dyes or a single dye, such as acridine orange. Measurement of morphologic changes might be useful for early cancer detection, where loss of tissue organization and enlarged nuclei are markers of dysplasia.

One issue of concern is that the dyes used in these experiments, AO and DiA, are not approved for use in humans. We are currently carrying out an animal safety study to assess the potential toxicity and mutagenicity of AO. Acriflavine hydrochloride, which is a homolog of AO, has been used for *in vivo* human imaging in Europe and Australia.[3] AO has also been used during photodynamic therapy to treat synovial sarcoma (soft tissue tumors) on human patients in Japan.[19]

There are clearly many applications of multispectral fluorescence measurement in biological monitoring and diagnosis. The multispectral imaging mode of the confocal microendoscope is a flexible and powerful feature of the system that will extend the range of applications as well as the system performance in those applications.

5 Conclusions

In this project, a confocal microendoscope system that can collect grayscale images in real time is upgraded by adding a multispectral imaging channel. The system is able to rapidly switch from grayscale imaging mode to collecting spatially resolved spectral information. Software to control the system and interactively display the multispectral information is also developed. The grayscale imaging mode of the confocal microendoscope has routinely provided high quality results and is currently involved in early stage *in vivo* clinical trials. The multispectral imaging mode of the confocal microendoscope produces excellent preliminary results. It has the same optical characteristics as the grayscale imaging mode in terms of spatial resolution, and enables the acquisition of high quality spatially localized spectra. The multispectral mode of the confocal microendoscope may be able to provide important diagnostic information *in vivo*. By using tissue or organelle-specific fluorophores with unique spectral properties, multispectral imaging can separate signal from different cellular compartments and provide unique diagnostic information.

References

1. K. Carlson, M. Chidley, K. B. Sung, M. Descours, A. Gillenwater, M. Follen, and R. Richards-Kortum, "*In vivo* fiber-optic confocal reflectance microscope with an injection-molded plastic miniature objective lens," *Appl. Opt.* **44**(10), 1792–1797 (2005).
2. K.-B. Sung, C. Liang, M. Descours, T. Collier, M. Follen, and R. Richards-Kortum, "Fiber-optic confocal reflectance microscope with miniature objective for *in vivo* imaging of human tissues," *IEEE Trans. Biomed. Eng.* **49**(10), 1168–1172 (2002).
3. R. Kiesslich, J. Burg, M. Vieth, J. Gnaendiger, M. Enders, P. Delaney, A. Polglase, W. McLaren, D. Janell, S. Thomas, B. Nafe, P. R. Galle, and M. F. Neurath, "Confocal laser endoscopy for diagnosing intraepithelial neoplasias and colorectal cancer *in vivo*," *Gastroenterology* **127**(3), 706–713 (2004).
4. A. Perchant, G. Le Goualher, M. Genet, B. Viellerobe, and F. Berier, "An integrated fibered confocal microscopy system for *in vivo* and *in situ* fluorescence imaging–applications to endoscopy in small animal imaging," in *Proc. IEEE Intl. Symp. Biomed. Imag. Nano to Macro*, pp. 692–695 (2004).
5. E. Laemmel, M. Genet, G. Le Goualher, A. Perchant, J. F. Le Gargasson, and E. Vicaut, "Fibered confocal fluorescence microscopy (Cell-viZio™) facilitates extended imaging in the field of microcirculation," *J. Vasc. Res.* **41**, 400–411 (2004).
6. L. Thiberville, S. Moreno-Swirc, T. Vercauteren, E. Peltier, C. Cavé, and G. Bourg-Heckly, "*In vivo* imaging of the bronchial wall microstructure using fibered confocal fluorescence microscopy," *Am. J. Resp. Crit. Care Med.* **175**, 22–31 (2007).
7. P. S. P. Thong, M. Olivo, K. W. Kho, W. Zheng, K. Mancer, M. Harris, and K. C. Soo, "Laser confocal endomicroscopy as a novel technique for fluorescence diagnostic imaging of the oral cavity," *J. Biomed. Opt.* **12**(1), 014007 (2007).
8. M. Goetz, A. Hoffman, P. R. Galle, M. F. Neurath, and R. Kiesslich, "Confocal laser endoscopy: new approach to the early diagnosis of tumours of the esophagus and stomach," *Future Oncol.* **2**(4), 469–476 (2006).
9. M. A. Brewer, U. Utzinger, J. K. Barton, J. B. Hoying, N. D. Kirkpatrick, W. R. Brands, J. R. Davis, K. Hunt, S. J. Stevens, and A. F. Gmitro, "Imaging of the ovary," *Technol. Cancer Res. Treat.* **3**(6), 617–627 (2004).
10. A. R. Rouse, A. Kano, J. A. Udovich, S. M. Kroto, and A. F. Gmitro, "Design and demonstration of a miniature catheter for a confocal microendoscope," *Appl. Opt.* **43**(31), 5763–5771 (2004).
11. A. R. Rouse, A. A. Tanbakuchi, J. A. Udovich, and A. F. Gmitro, "Design of an *in vivo* multi-spectral confocal microendoscope for clinical trials," *Proc. SPIE* **6082**, 15–22 (2006).
12. Y. S. Sabharwal, A. R. Rouse, L. Donaldson, M. F. Hopkins, and A. F. Gmitro, "Slit-scanning confocal microendoscope for high resolution *in vivo* imaging," *Appl. Opt.* **38**(34), 7133–7144 (1999).
13. A. R. Rouse and A. F. Gmitro, "Multispectral imaging with a confocal microendoscope," *Opt. Lett.* **25**(23), 1708–1710 (2000).
14. A. R. Rouse, J. A. Udovich, and A. F. Gmitro, "*In vivo* multi-spectral confocal microscopy," *Proc. SPIE* **5701**, 73–84 (2005).
15. F. Jean, G. Bourg-Heckly, and B. Viellerobe, "Fibered confocal spectroscopy and multicolor imaging system for *in vivo* fluorescence analysis," *Opt. Express* **15**(7), 4008–4017 (2007).
16. C. Millot, J. M. Millot, H. Morjani, A. Desplaces, and M. Manfait, "Characterization of acidic vesicles in multidrug-resistant and sensitive cancer cells by acridine orange staining and confocal microspectrofluorometry," *J. Histochem. Cytochem.* **45**(9), 1255–1264 (1997).
17. J. Kapuscinski, Z. Darzynkiewicz, and M. R. Melamed, "Interactions of acridine orange with nucleic acids. Properties of complexes of acridine orange with single stranded ribonucleic acid," *Biochem. Pharmacol.* **32**, 3679–3694 (1983).
18. A. V. Zelenin, "Fluorescence microscopy of lysosomes and related structures in living cells," *Nature (London)* **212**, 425–426 (1966).
19. K. Kusuzaki et al., "Clinical outcome of a novel photodynamic therapy technique using acridine orange for synovial sarcomas," *Photochem. Photobiol.* **81**, 705–709 (2005).